

Article

Synergistic Effects of Boron and Rare Earth Elements on the Microstructure and Stress Rupture Properties in a Ni-Based Superalloy

Qiang Tian ¹, Shuo Huang ^{1,*}, Heyong Qin ¹, Ran Duan ¹, Chong Wang ² and Xintong Lian ^{3,*}

¹ Central Iron and Steel Research Institute Co., Ltd., Beijing 100081, China; qtian1frank@163.com (Q.T.); qinheyong@126.com (H.Q.); duanran@cisri-gaona.com.cn (R.D.)

² School of Materials Science and Engineering, Northeastern University, Shenyang 110819, China; 2190025@stu.neu.edu.cn

³ School of Materials Science and Engineering, Shanghai University, Shanghai 200444, China

* Correspondence: huangshuohank@163.com (S.H.); xtlian@shu.edu.cn (X.L.)

Abstract: The synergistic effects of boron (B) and rare earth (RE) elements on the microstructure and stress rupture properties were investigated in a Ni-based superalloy. The stress rupture lifetime at 650 °C/873 MPa significantly increased with the addition of B as a single element. Furthermore, the stress rupture lifetime reached its peak (303 h), with a certain amount of B and RE added together in test alloys. Although the grain size and morphology of the γ' phase varied a little with the change in B and RE addition, they were not considered to be the main reasons for stress rupture performance. The enhancement in stress rupture lifetime was mostly attributed to the segregation of the B and RE elements, which increased the binding force of the grain boundary and improved its strength and plasticity. In addition, the enrichment of B and RE inhabited the precipitation of carbides along grain boundaries. Furthermore, nano-scale RE precipitates containing sulfur (S) and phosphorus (P) were observed to be distributed along the grain boundaries. The purification of grain boundaries by B and RE elements was favorable to further improve the stress rupture properties.

Keywords: Ni-based superalloy; boron; rare earth; element segregation; stress rupture life



Citation: Tian, Q.; Huang, S.; Qin, H.; Duan, R.; Wang, C.; Lian, X.

Synergistic Effects of Boron and Rare Earth Elements on the Microstructure and Stress Rupture Properties in a Ni-Based Superalloy. *Materials* **2024**, *17*, 2007. <https://doi.org/10.3390/ma17092007>

Academic Editor: Sergey V. Zherebtsov

Received: 17 March 2024

Revised: 19 April 2024

Accepted: 23 April 2024

Published: 25 April 2024



Copyright: © 2024 by the authors. Licensee MDPI, Basel, Switzerland. This article is an open access article distributed under the terms and conditions of the Creative Commons Attribution (CC BY) license (<https://creativecommons.org/licenses/by/4.0/>).

1. Introduction

Nickel-based superalloys have been considered as a kind of promising metal for high-temperature structure components in the field of aerospace, especially used for gas turbine components due to their outstanding comprehensive mechanical properties [1–4]. Superalloys, such as GH4169, GH4706 and GH4742, are commonly used in gas turbine engines under the conditions of extreme heat exposure. Among these superalloys, the GH4742 alloy is a typical Ni-Cr-Co-based superalloy, strengthened by the precipitation of the γ' phase with a high content of Al, Ti and Nb. The total content of alloying strengthening elements is more than 7.8%, which are the forming elements of the γ' phase. After heat treatment, the content of the γ' phase can reach 35%. Moreover, the GH4742 alloy has good high-temperature properties due to the solution-strengthening effect of Mo, Co and the grain-strengthening effect of microalloying elements like rare earth elements and B. Based on its special chemical components, the strength of the GH4742 alloy can exceed 1300 MPa under room temperature and 1000 MPa under 700 °C. The process of the GH4742 alloy usually consists of double vacuum melting (VIM+VAR), forging cogging and hot die forging forming, which can ensure the purity of this material. Therefore, the GH4742 alloy has been widely used in high-temperature components, for instance, high-pressure turbine discs under a service temperature of 750–800 °C [5,6].

As technology develops, new-type gas turbines put forward higher service performance requirements for their rotating high-pressure turbine discs. The service life of the

GH4742 alloy high-pressure turbine disc is expected to be increased from more than 50 h at 650 °C/823 MPa to more than 50 h at 650 °C/873 MPa without increasing the upper limit of hardness. It is known that three traditional methods can be used to improve the service life, including controlling the grain size by reasonably forging and the use of heat treatment, strengthening the precipitated phase with a certain size and distribution through the heat treatment system and strengthening the grain boundary by microalloying [7–10]. Among these, recent studies have concentrated on optimizing superalloys by employing the potential precipitation and solute effect of microalloying elements, which makes it possible to precisely control the microstructure and maximally optimize the performance. For instance, B is one of the most widely used trace elements in superalloys, with remarkable influence on prolonging long-time properties, such as stress rupture and creep life, and inhibiting fatigue crack propagation [11–13]. Researchers have found that the segregation of boron (B) can decrease the energy of the grain boundary and affect its diffusion [14,15]. Previous studies have also investigated the addition of B in some Ni-based superalloys, which can modify the morphologies and distribution precipitates along grain boundaries, such as the δ phase, η phase, carbides or even Laves phase, thus enhancing the stress rupture properties [16]. Recently, rare earth (RE) elements have been regarded as promising alloying elements for nickel-based superalloys due to their effects on strengthening the grain boundary and promoting solid solution strengthening [17–19]. RE elements have been applied successfully in many metallurgy fields to improve the mechanical performance of materials and oxidation resistance properties of nickel-based superalloys [20–23].

In this study, the synergistic effects of B and RE elements on the microstructure and stress rupture properties were investigated and discussed. The existing forms of these trace elements in the alloy were further studied and confirmed accurately by the utilized characterization methods of transmission electron microscope (TEM), electron probe microanalysis (EPMA) and Auger electron spectroscopy (AES). This study concludes with a brief discussion of the experimental results, which will establish the theoretical basis of B and RE microalloying and provide guidance for the application of GH4742 alloy or other types of superalloys.

2. Materials and Methods

The chemical compositions (weight, %) of GH4742 alloy used in this study were detected by SPECTRO MAX 6 (Kleve, Germany) direct-reading spectrometry, as shown in Table 1. The ingots with a diameter of 150 mm were obtained by vacuum induction melting (VIM) and vacuum arc remelting (VAR). After homogenizing for 72 h at 1135 °C and forging at 1100 °C, a certain size of turbine disc forging was prepared. Then, being treated through heat treatment processes of 1120 °C \times 8 h (air cooling) + 780 °C \times 16 h (air cooling), the samples were evaluated by means of microstructure characterization and mechanical property testing.

Table 1. Chemical compositions of GH4742 alloys (wt.%).

Sample	Cr	Co	Mo	Al	Nb	Ti	Fe	C	B	La	Ce	Ni
Alloy 1	14.09	9.82	5.04	2.73	2.75	2.71	0.031	0.059	0.0005	0.009	0.001	Bal.
Alloy 2	14.04	9.78	5.00	2.71	2.72	2.72	0.065	0.048	0.004	0.009	0.001	Bal.
Alloy 3	13.99	9.90	5.02	2.72	2.66	2.68	0.064	0.048	0.007	0.007	0.001	Bal.
Alloy 4	14.05	9.84	5.06	2.72	2.73	2.68	0.069	0.052	0.007	0.016	0.002	Bal.
Alloy 5	14.03	9.84	5.07	2.76	2.73	2.69	0.078	0.055	0.008	0.034	0.005	Bal.

The microstructure was measured by Olympus GX71 (Tokyo, Japan) optical microscope (OM), JEOL JSM-7800F (Tokyo, Japan) scanning electron microscope (SEM) and FEI Talos F200X (Waltham, MA, USA) transmission electron microscope (TEM) to observe the evolution of grain and precipitation. Image-Pro Plus 6.0 software was used for quantitative statistics of grain and second phase, and the number of γ' phases was more than 100. The samples were etched using a solution of 20 g CuCl_2 + 100 mL HCl + 100 mL $\text{C}_2\text{H}_5\text{OH}$ for

particles were found to be located between square primary γ' phases, which were likely to be precipitated during the subsequent aging treatment. From the SEM results above, the addition of B and RE seemed to have no significant effects on the size and morphology of the γ' phase.

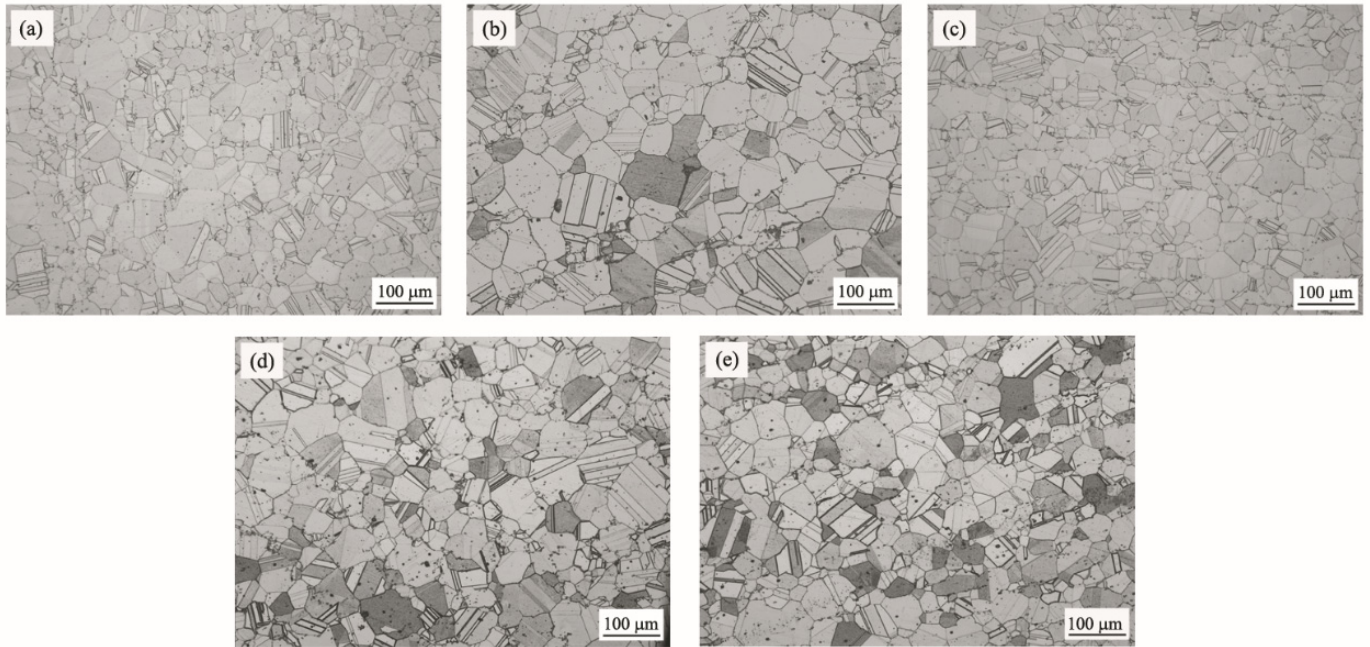


Figure 2. Microstructure of different GH4742 test alloys: (a) alloy 1; (b) alloy 2; (c) alloy 3; (d) alloy 4; (e) alloy 5.

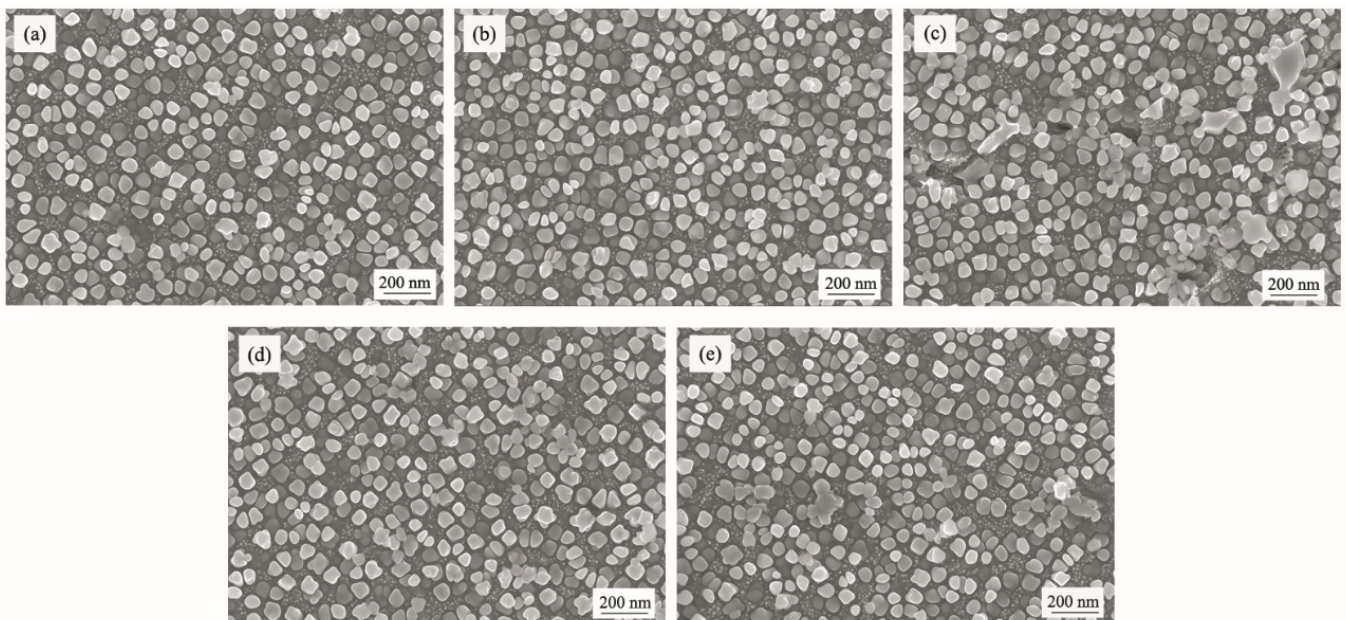


Figure 3. SEM images of γ' phase of different GH4742 test alloys: (a) alloy 1; (b) alloy 2; (c) alloy 3; (d) alloy 4; (e) alloy 5.

In order to show the synergistic effects of RE and B on precipitates, EPMA was applied to observe the morphology and measure the element distribution of precipitates. The results in test alloy 5 are shown in Figure 4. Large amounts of carbides containing C, Nb, Ti and B elements were observed to be precipitated at the grain boundaries. In addition, fine

spherical or ellipsoidal RE compounds containing La, Ce and P elements were found to be distributed with a size of less than 2 μm near the grain boundaries. The results above showed that after B and RE alloying, B and RE may combine with small amounts of other elements to form more complicated oxides, sulfides or complex inclusions.

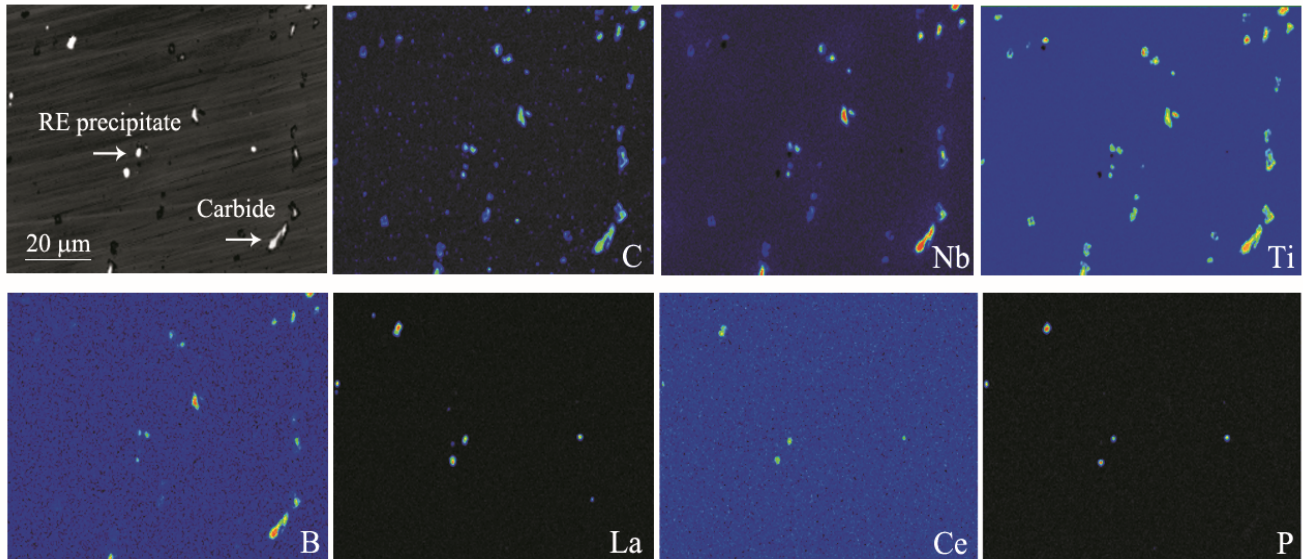


Figure 4. EPMA images of element distribution in precipitate towards grain boundary in alloy 5.

3.2. Effects of B and RE Elements on Stress Rupture Properties

The results of stress rupture properties are given in Table 2 and Figure 5. It was indicated that the addition of B as a single element significantly increased the stress rupture life from 8 h (alloy 1) to 189 h (alloy 3). When a certain amount of RE elements was added to the test alloys, the synergistic effects of B and RE were fully exerted, showing that the stress rupture life had improved to 237 h (alloy 4) and 303 h (alloy 5), respectively. Therefore, a combination of B and RE can significantly improve the stress rupture properties.

Table 2. Stress rupture properties of GH4742 alloys at 650 °C/873 MPa.

Sample	Stress Rupture Life (h)	Elongation (%)
Alloy 1	8	2.8
Alloy 2	123	2.9
Alloy 3	189	2.3
Alloy 4	237	2.7
Alloy 5	303	2.7

Figure 6 shows the fracture surface morphology of the tested stress rupture samples. The failure mode in test alloy 1 and alloy 2 was typically intergranular (Figure 6a,b). The whole surfaces were flat and composed of intergranular cracks. At higher magnification, a large number of secondary cracks were observed on the fracture surfaces, indicating that the strength of the grain boundary was lower than the intergranular strength (Figure 6k,l). In alloy 3, the minor intergranular fracture zone was found around the specimen edge (Figure 6c), while the center part was determined as the transgranular fracture zone with a certain amount of cleavage steps (Figure 6h,m). It was indicated that the mixed fracture mode was dominated in test alloy 3. With the addition of the RE element, the area covered by a transgranular fracture was further expanded in alloy 4 (Figure 6d,e), and, furthermore, the entire surface was fully covered by cleavage steps in alloy 5 (Figure 6j,o). Pictures with high magnification display that there was a small amount of carbon or nitride around the crack source, showing that the cracks begin with precipitates instead of the grain boundary.

As a result, the fracture modes converted from intergranular fracture mode to transgranular fracture mode with increasing contents of B and RE due to the effects on improving the grain boundary strength.

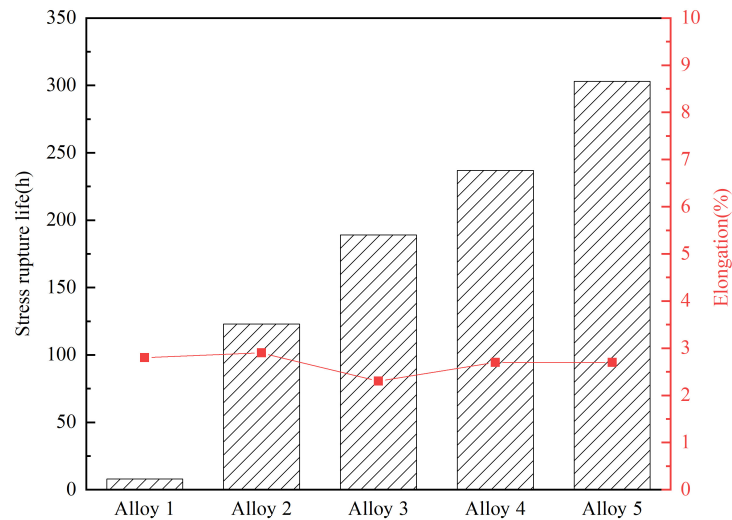


Figure 5. Stress rupture properties of different GH4742 test alloys.

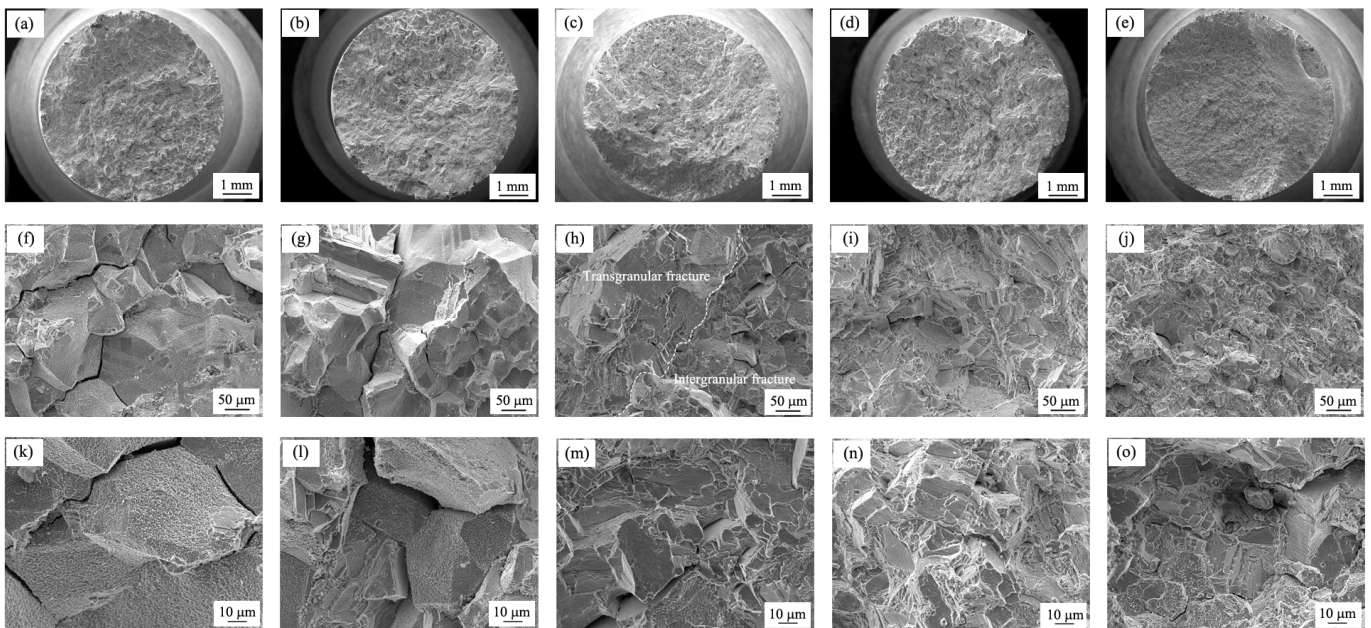


Figure 6. Morphologies of fracture surface of test alloys: (a,f,k) alloy 1; (b,g,l) alloy 2; (c,h,m) alloy 3; (d,i,n) alloy 4; (e,j,o) alloy 5.

4. Discussion

4.1. Effects of Microstructure on Stress Rupture Properties

Similar to other superalloys, the grain size of the GH4742 alloy under the premise of the same alloying elements is the main issue affecting the tensile properties at room temperature and stress rupture properties at high temperature. Grain refinement is an effective strengthening method in engineering applications. Compared with other strengthening methods, fine grain strengthening is the only way that increases both the strength and plasticity of materials. However, the precondition of fine grain strengthening is that the grain boundary impedes dislocation slip, which exists at a low temperature. For the GH4742 alloy, the grain boundary is essentially a defect when the temperature rises. With

the strengthening of atomic activity, the grain boundary also becomes unstable, which will lead to a weakened grain boundary. Therefore, proper grain coarsening is beneficial in improving the stress rupture performance.

Coherent stress strengthening is an important aspect of γ' phase strengthening, which can influence the dislocation behavior by dispersing in the matrix to achieve alloy strengthening. The γ' phase, as a strengthening phase for superalloys, has a significant impact on the stress rupture properties. The increase in the content of the γ' phase and the decrease in size are beneficial for improving the fatigue performance and creep resistance of nickel-based superalloys. The increasing content of the γ' phase will result in excellent stress rupture properties.

The two influencing factors above play a role in the premise that the alloy composition is unchanged. However, in this study, the influence of alloying elements on the properties is significantly greater than that of these two factors. Therefore, the changes in grain size and γ' phase are not the main reasons for improving the stress rupture properties.

4.2. Effects of B and RE Elements on Stress Rupture Properties

Due to the different atomic size and chemical properties between Ni and trace elements, B and RE tend to segregate towards grain boundaries. In order to study element segregation more clearly, five equidistant areas close to the grain boundary were selected for quantitative analysis. A schematic diagram of the selected areas and the AES spectrum are shown in Figure 7. From the results above, the element content was accurately characterized. Table 3 shows the distribution of elements at different positions from grain boundaries in test alloy 5. It can be seen that the content of B in Area 1 near the grain boundary was the highest (6.02%), and the content of B gradually decreased to 4.89% (Area 2), 0.70% (Area 3) and 0.01 (Area 4 and Area 5) as the distance from the grain boundary increased. Although the content of B was not very accurate due to its low addition, it was fully proved that the segregation of B towards the grain boundary was strong. The content of C in Area 1 was also high (13.33%), and the content of C decreased significantly as the distance from the grain boundary increased. The contents of Nb and Ti near the grain boundary were also high, which indicated that carbides precipitated along the grain boundaries. In contrast, the contents of Al, Cr and Co near the grain boundary were much lower than those in the grain, making it clear that these three elements were depleted along the grain boundaries. The contents of Mo and Ti changed minimally. It is noteworthy that no effective contents of RE were detected due to the trace contents.

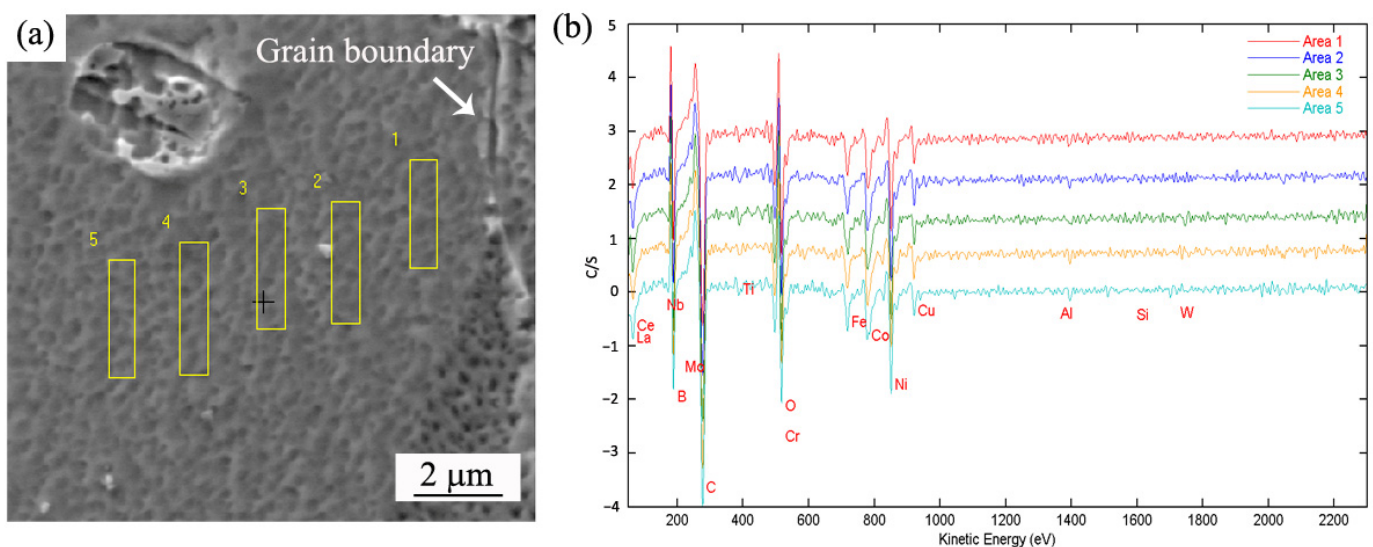
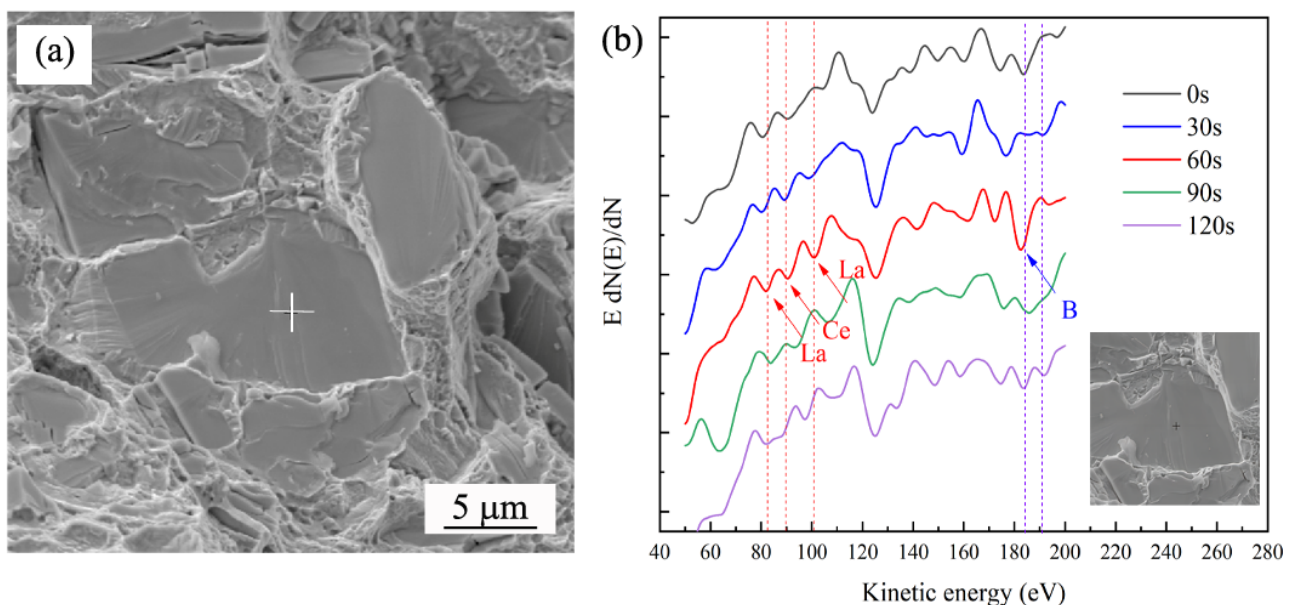


Figure 7. A schematic diagram of selected areas (a) and its AES spectrum (b) in alloy 5.

Table 3. AES analysis results in test alloy 5 (wt.%).

Element	C	B	Mo	Ti	Nb	Al	Cr	Co	Ni
Area 1	13.33	6.02	3.43	1.24	5.17	0.93	4.61	4.56	Bal.
Area 2	10.49	4.89	3.56	2.33	4.45	1.61	6.57	5.70	Bal.
Area 3	0.57	0.70	3.60	2.34	2.45	1.89	8.83	9.49	Bal.
Area 4	0.12	0.01	4.11	2.24	2.41	2.77	13.76	9.20	Bal.
Area 5	0.093	0.01	4.20	2.51	2.65	2.65	13.58	9.06	Bal.

Due to the particularity of RE and the fact that the content of RE was not detected in the full spectrum in Figure 7, we designed a specific experiment. A special intergranular fracture surface was prepared, and the variation in the RE and B content sputtered at different times was measured. The AES spectrum in Figure 8 proves the segregation of B and RE elements in alloy 5. Reports have shown that the kinetic energy range of Ce and La is from 52 eV to 115 eV. Typical Auger peaks of La (64 eV, 83 eV and 99 eV) and Ce (68 eV, 87 eV and 104 eV) were chosen for detection. The Auger peak of B was at 185 eV. The change in the inner energy level was caused by the transfer of atomic charge, thus changing the energy of the Auger transition and leading to the displacement of Auger peaks [25,26]. The spectra lines had a minor difference compared to the standard peaks in the Auger Electron Spectroscopy Reference Manual [27].

**Figure 8.** Intergranular fracture morphology (a) and AES spectrum of La, Ce and B (b) in alloy 5.

Due to the existence of high-temperature oxidation, the surface oxygen content was higher when the sputtering time was 0 s and 30 s, and no element segregation was found on the surface. After sputtering for 60 s, some typical peaks of RE and B elements were detected. The tested Auger peak of Ce was at 90 eV, and the tested Auger peaks of La were at 82 eV and 100 eV. Some studies have displayed that RE atoms tend to be enriched at grain boundaries because of their large radius [28,29]. The results above confirmed that Ce and La atoms gathered at the surface of the fracture samples. The same was true for B (the peak was determined at 183 eV), which segregated towards grain boundaries. After sputtering for 90 s, the peak values of peaks disappeared gradually, which indicated that the contents of RE and B elements were decreasing. After sputtering for 120 s, the peaks disappeared totally because the contents of RE and B were too low to detect.

The results above show that the B and RE elements significantly segregated towards the grain boundaries. Moreover, these two kinds of elements usually exist in the form of

the atomic state, affecting the distribution of other elements at the grain boundary [15,29]. In the grain boundary regions, where the atomic order is relatively chaotic and the energy is high, B and RE atoms can occupy the vacancies of the grain boundary and improve the interface bonding force, which is considered the main reason for improving the long-time performance.

Figure 9 manifested two types of precipitates along grain boundaries and their corresponding EDS mappings. The results showed that the nano-scale continuous irregular stirps were enriched with Ce, O and Cr, indicating that the precipitate was an RE compound with a size of less than 500 nm (Figure 9a). Another precipitate was determined as a complex inclusion containing C, B, La, P and S, with an irregular bulk shape (Figure 9b). It was seemingly confirmed that RE elements tend to combine with O and S preferentially, which coincides with the results of a previous study [30,31].

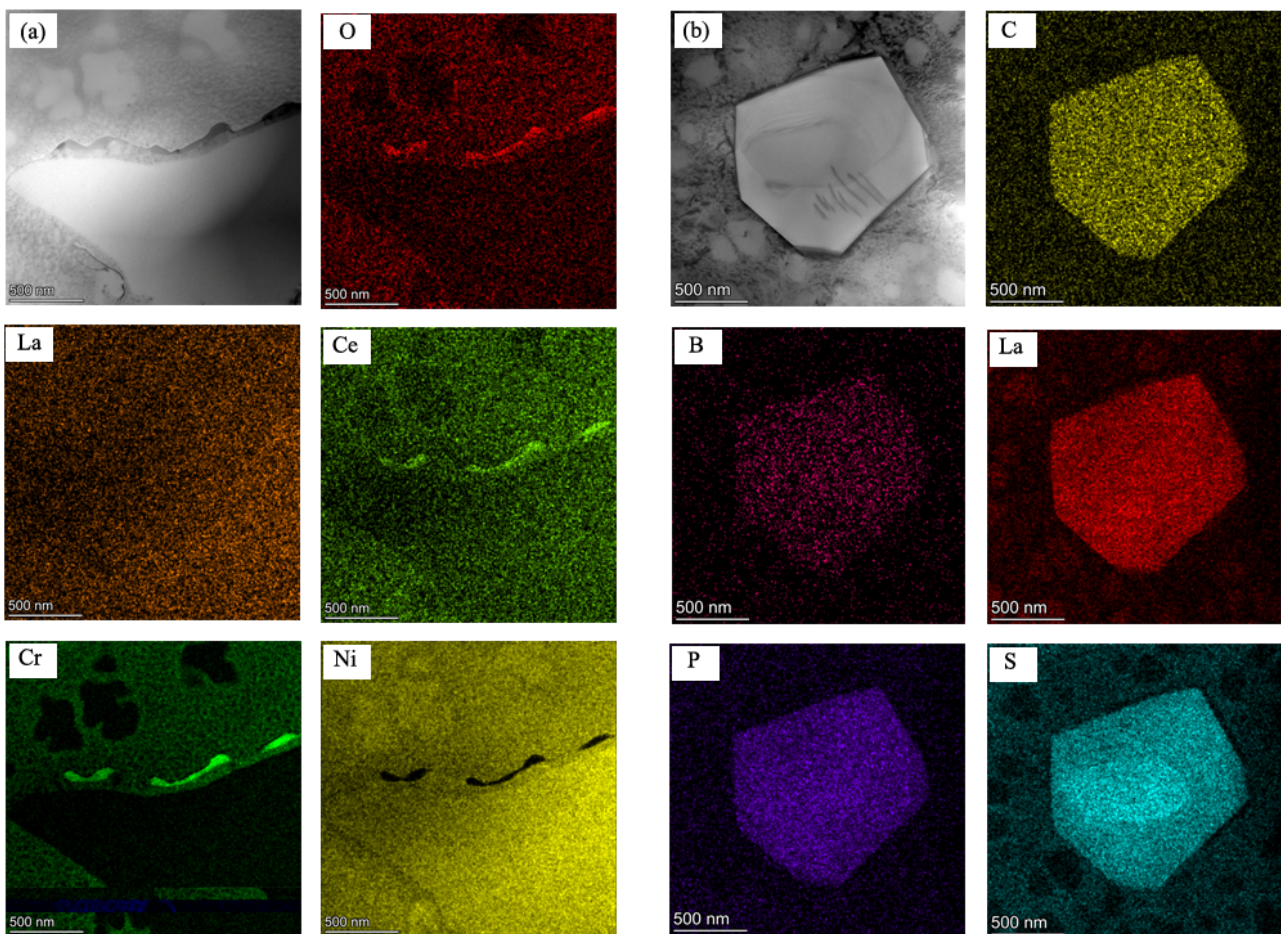


Figure 9. STEM-HAADF images and elemental mapping of grain boundary precipitates in alloy 5 (a) RE compound with Ce, O and Cr (b) RE complex inclusion with C, B, La, P and S.

Based on previous research, the nano-scale precipitates had no obvious detrimental effect on the mechanical properties [32–34]. When Ce was added to the GH4742 alloy, it seemed to form a compound with a higher melting point, with the original compound showing a lower melting point, thus strengthening the grain boundaries and improving the stress rupture properties.

In addition to stable enrichment at the grain boundaries, La could also form complex inclusions with carbides, which contained P and S elements. P and S were considered to be detrimental impurity elements because of the tendency to segregate towards grain boundaries [35]. Based on the theory of segregation, the impurity elements gathering towards interfaces could weaken grain boundaries and, thus, result in brittle

fracture [36,37]. Thereby, the formation of complicated RE precipitates could reduce the segregation of harmful elements towards grain boundaries, playing a purification role and, thus, improving the instantaneous and durable properties of the GH4742 superalloy. However, excess content of La formed Ni₅La along the grain boundaries, reducing the stress rupture properties of the alloy based on a previous study [38]. No Ni₅La was formed in this study, because the amount of lanthanum was strictly controlled to ensure that it does not exceed the limit.

The atomic radius of B was larger than that of C. The addition of B could reduce the creep rate, improve the sensitivity of permanent notch and increase the high-temperature plasticity of the alloy. The segregation and precipitation of B towards the grain boundaries made it difficult for carbides such as cellular M₂₃C₆ or bulk MC to precipitate and improve the grain boundary state. However, adding too much B may form more B compounds on the grain boundary, which will reduce the workability and plasticity of the alloy [39].

Generally, the segregation of B and RE towards grain boundaries and the synergistic effect with other elements were confirmed based on the investigated data above. As P and S elements were contained in the B and RE precipitates near grain boundaries, the degree of impurity element segregation towards grain boundaries was substantially reduced. This could provide strong evidence that the purification of grain boundaries eliminated the stress concentration, thus leading to an improvement in the stress rupture life. The importance of grain boundary purification was also proved. Therefore, the synergistic effect of B and RE cannot be ignored.

5. Conclusions

In this study, the synergistic effects of boron (B) and rare earth (RE) elements on the microstructure and stress rupture properties were studied. The stress rupture properties at 650 °C/873 MPa significantly increased with the addition of B and RE. The grain size and the morphology of the γ' phase were not the main reasons for improving the stress rupture properties. The enhancement in the stress rupture lifetime was mostly attributed to the segregation of B and RE towards grain boundaries, which increased the binding force of the grain boundary and improved its strength and plasticity. In addition, the enrichment of B and RE inhibited the precipitation of carbides along grain boundaries. Furthermore, two types of RE precipitate containing S and P were found along grain boundaries. The purification of grain boundaries by the B and RE elements was beneficial to the enhancement of stress rupture properties.

The successful development of new GH4742 using the method of microalloying support for the reserve as new materials lays a firm foundation for the development of other superalloys that are hard to deform.

Author Contributions: Funding acquisition, H.Q. and S.H.; formal analysis, R.D.; investigation, Q.T. and C.W.; writing—original draft preparation, Q.T.; writing—review and editing, X.L. All authors have read and agreed to the published version of the manuscript.

Funding: This work was financially supported by the National Key Research and Development Program of China (2022YFB3705105).

Institutional Review Board Statement: Not applicable.

Informed Consent Statement: Not applicable.

Data Availability Statement: Data are contained within this article.

Conflicts of Interest: Authors Qiang Tian, Shuo Huang, Heyong Qin and Ran Duan were employed by the company Central Iron and Steel Research Institute Co., Ltd. The remaining authors declare that the research was conducted in the absence of any commercial or financial relationships that could be construed as a potential conflict of interest.

References

1. Osada, T.; Nagashima, N.; Gu, Y.F.; Yuan, Y.; Yokokawa, T.; Harada, H. Factors contributing to the strength of a polycrystalline nickel-cobalt base superalloy. *Scr. Mater.* **2011**, *64*, 892–895. [\[CrossRef\]](#)
2. Utada, S.; Sasaki, R.; Reed, R.C.; Tang, Y.T. Overheating of Waspaloy: Effect of cooling rate on flow stress behavior. *J. Mater. Design* **2022**, *221*, 110911. [\[CrossRef\]](#)
3. Amiri, A.; Bruschi, S.; Sadeghi, M.H.; Bariani, P. Investigation on hot deformation behavior of Waspaloy. *Mater. Sci. Eng. A* **2013**, *562*, 77–82. [\[CrossRef\]](#)
4. Devaux, A.; Georges, E.; Heritier, P. Development of New C&W Superalloys for High Temperature Disk Applications. *Adv. Mater. Res.* **2011**, *278*, 405–410.
5. Kong, W.W.; Wang, Y.Q.; Chen, Y.P.; Liu, X.; Yuan, C. Investigation of uniaxial ratcheting fatigue behaviours and fracture mechanism of GH742 superalloy at 923K. *Mater. Sci. Eng. A* **2022**, *831*, 142173. [\[CrossRef\]](#)
6. Zhang, F.Z.; Wang, C.S.; Wu, Y.S.; Zhou, L.Z.; Tian, Q. Microstructural stability and mechanical properties of GH742 Ni-based wrought superalloy for turbine disk applications. *Mater. Sci. Eng. A* **2022**, *832*, 142488. [\[CrossRef\]](#)
7. Sharma, J.; Nicolaÿ, A.; Graef, M.D.; Bozzolo, B. Phase discrimination between δ and η phases in the new nickel-based superalloy VDM Alloy 780 using EBSD. *Mater. Charact.* **2021**, *176*, 111105. [\[CrossRef\]](#)
8. Sharghi-Moshtaghin, R.; Asgari, S. The influence of thermal exposure on the γ' precipitates characteristics and tensile behavior of superalloy IN-738LC. *J. Mater. Process. Technol.* **2004**, *147*, 343–350. [\[CrossRef\]](#)
9. Theska, F.; Street, S.R.; Lison-Pick, M.; Primig, S. Grain boundary microstructure-property relationships in the cast & wrought Ni-based superalloy René 41 with boron and carbon additions. *Acta Mater.* **2023**, *258*, 119235.
10. Zheng, L.; Xu, T.D.; Deng, Q.; Dong, J.X. Experimental study on the characteristic of grain-boundary segregation of phosphorus in Ni-base superalloy. *Mater. Lett.* **2008**, *62*, 54–56. [\[CrossRef\]](#)
11. Wang, C.S.; Guo, Y.A.; Guo, J.T.; Zhou, L.Z. Investigation and improvement on structural stability and stress rupture properties of a Ni-Fe based alloy. *Mater. Sci. Eng. A* **2015**, *88*, 790–798. [\[CrossRef\]](#)
12. Antonov, S.; Després, A.; Mayer, C.; Martin, G.; Kontis, P. Boron trapping at dislocations in an additively manufactured polycrystalline superalloy. *J. Mater. Eng. Perform.* **2023**, *30*, 101801. [\[CrossRef\]](#)
13. Stinville, J.C.; Gallup, K.; Pollock, T.M. Transverse Creep of Nickel-Base Superalloy Bicrystals. *Metall. Mater. Trans. A* **2015**, *46*, 2516–2529. [\[CrossRef\]](#)
14. Sanyal, S.; Waghmare, U.V.; Subramanian, P.R.; Gigliotti, M.F.X. Effect of dopants on grain boundary decohesion of Ni: A first-principles study. *Appl. Phys. Lett.* **2008**, *93*, 223113. [\[CrossRef\]](#)
15. Zhou, P.J.; Yu, J.J.; Sun, X.F.; Guan, H.R.; Hu, Z.Q. The role of boron on a conventional nickel-based superalloy. *Mater. Sci. Eng. A* **2008**, *491*, 159–163. [\[CrossRef\]](#)
16. Kontis, P.; Mohd Yusof, H.A.; Pedrazzini, S.; Danaie, M.; Moore, K.L.; Bagot, P.A.J.; Moody, M.P.; Grovenor, C.R.M.; Reed, R.C. On the effect of boron on grain boundary character in a new polycrystalline superalloy. *Acta Mater.* **2016**, *103*, 688–699. [\[CrossRef\]](#)
17. Dhakar, B.M.; Dwivedi, D.K.; Sharma, S.P. Studies on remelting of tungsten carbide and rare earth modified nickel base alloy composite coating. *Surf. Eng.* **2012**, *28*, 73–80. [\[CrossRef\]](#)
18. Palleda, T.N.; Chowdhury, H.T.; Banoth, S.; Murakami, H.; Kakehi, K. Effects of yttrium content on solidification, microstructure, and mechanical properties of laser powder bed fused IN718 superalloy. *J. Alloys Compd.* **2022**, *918*, 165763. [\[CrossRef\]](#)
19. Park, C.W.; Byun, J.M.; Choi, W.J.; Lee, S.Y.; Kim, Y.D. Improvement of high temperature mechanical properties of Ni-based oxide dispersion strengthened alloys by preferential formation of Y-Ti-O complex oxide. *Mater. Sci. Eng. A* **2019**, *740–741*, 363–367. [\[CrossRef\]](#)
20. Oh, Y.; Han, C.H.; Wang, M.; Chun, Y.B.; Han, H.N. Effect of rare earth oxide addition on microstructure and mechanical properties of Ni-based alloy. *J. Alloys Compd.* **2021**, *853*, 156980. [\[CrossRef\]](#)
21. Ding, M.Q.; Hu, P.; Ru, Y.; Zhao, W.Y.; Pei, Y.L.; Li, S.S.; Gong, S.K. Effects of rare-earth elements on the oxidation behavior of γ -Ni in Ni-based single crystal superalloys: A first principles study from a perspective of surface adsorption. *Appl. Surf. Sci.* **2021**, *547*, 149173. [\[CrossRef\]](#)
22. Guimarães, A.V.; Silveira, R.M.S.; Jaffrezou, N.; Mendes, M.C.; Santos, D.S.; Almeida, L.H.; Araujo, L.S. Influence of yttrium alloying on improving the resistance to hydrogen embrittlement of superalloy 718. *Int. J. Hydrogen Energy* **2024**, *58*, 479–484. [\[CrossRef\]](#)
23. Rong, L.R.; Wang, M.; Xing, W.W.; Hao, X.C.; Ma, Y.C. Effects of cerium addition on the microstructure and stress rupture properties of a new nickel-based cast superalloy. *J. Mater. Sci. Technol.* **2023**, *159*, 112–124. [\[CrossRef\]](#)
24. GB/T 2039-2012; Metallic Materials—Uniaxial Creep Testing Method in Tension. Standards Press of China: Beijing, China, 2012.
25. Liu, Z.; Lian, X.T.; Liu, T.S.; Yang, Y.D.; Zhu, J.N.; Dong, H. Effects of rare earth elements on corrosion behaviors of low-carbon steels and weathering steels. *Mater. Corros.* **2020**, *71*, 258–266. [\[CrossRef\]](#)
26. Lian, X.T.; Zhu, J.N.; Wang, R.Q.; Liu, T.S.; Xu, J.; Xu, D.X.; Dong, H. Effects of Rare Earth (Ce and La) on Steel Corrosion Behaviors under Wet-Dry Cycle Immersion Conditions. *Metals* **2020**, *71*, 1174. [\[CrossRef\]](#)
27. McGuire, G. Cesium. In *Auger Electron Spectroscopy Reference Manual*; Springer: Boston, MA, USA, 1979; pp. 114–116.
28. Guo, Y.; Sun, S.F.; Song, S.H. Effect of minor rare earth cerium addition on the hot ductility of a reactor pressure vessel steel. *Results Phys* **2019**, *15*, 102746. [\[CrossRef\]](#)

29. Barrett, G.E.; Imandoust, A.; Kadiri, H.E. The effect of rare earth element segregation on grain boundary energy and mobility in magnesium and ensuing texture weakening. *Scr. Mater.* **2018**, *146*, 46–50. [[CrossRef](#)]
30. Deng, X.X.; Jiang, M.; Wang, X.H. Mechanisms of inclusion evolution and intra-granular acicular ferrite formation in steels containing rare earth elements. *Acta Metall. Sin. (Engl. Lett.)* **2012**, *25*, 241–248.
31. Wu, Y.M.; Wang, L.M.; Du, T. Thermodynamics of rare earth elements in liquid iron. *J. Less-Common Met.* **1985**, *110*, 187–193. [[CrossRef](#)]
32. Hou, D.W.; Fang, F.; Wang, Y.; Zhang, Y.X.; Zhang, X.M.; Misra, R.D.K.; Yuan, G. Nanoprecipitation behavior and resultant mechanical and magnetic properties in Fe-Si-Ni-Al-Mn high strength non-oriented silicon steel. *Mater. Sci. Eng. A* **2021**, *819*, 141529. [[CrossRef](#)]
33. Hu, J.; Du, L.X.; Xu, W.; Zhai, J.H.; Dong, Y.; Liu, Y.J.; Misra, R.D.K. Ensuring combination of strength, ductility and toughness in medium manganese steel through optimization of nano-scale metastable austenite. *Mater. Charact.* **2018**, *136*, 20–28. [[CrossRef](#)]
34. Lian, X.T.; Chen, L.; Fan, Z.W.; Liu, T.S.; Xu, D.X.; Dong, H. Effects of Modified Inclusions and Precipitates Alloyed by Rare Earth Element on Corrosion and Impact Properties in Low Alloy Steel. *Acta Metall. Sin. (Engl. Lett.)* **2022**, *35*, 1719–1730. [[CrossRef](#)]
35. Wang, L.M.; Lin, Q.; Yue, L.J.; Liu, L.; Guo, F.; Wang, F.M. Study of application of rare earth elements in advanced low alloy steels. *J. Alloys Compd.* **2008**, *451*, 534–537. [[CrossRef](#)]
36. Gibson, M.A.; Schuh, C.A. Segregation-induced changes in grain boundary cohesion and embrittlement in binary alloys. *Acta Mater.* **2015**, *95*, 145–155. [[CrossRef](#)]
37. Tervo, H.; Kaijalainen, A.; Pikkarainen, T.; Mehtonen, S.; Porter, D. Effect of impurity level and inclusions on the ductility and toughness of an ultra-high-strength steel. *Mater. Sci. Eng. A* **2017**, *697*, 184–193. [[CrossRef](#)]
38. Song, X.; Wang, L.; Liu, Y.; Ma, H.P. Effects of temperature and rare earth content on oxidation resistance of Ni-based superalloy. *Prog. Nat. Sci.* **2011**, *21*, 227–235. [[CrossRef](#)]
39. Garosshen, T.J.; Tillman, T.D.; McCarthy, G.P. Effects of B, C, and Zr on the structure and properties of a P/M nickel base superalloy. *Metall. Trans. A* **1987**, *18*, 69–77. [[CrossRef](#)]

Disclaimer/Publisher’s Note: The statements, opinions and data contained in all publications are solely those of the individual author(s) and contributor(s) and not of MDPI and/or the editor(s). MDPI and/or the editor(s) disclaim responsibility for any injury to people or property resulting from any ideas, methods, instructions or products referred to in the content.